Molecular Therapy
Oncology
Original Article

A tri-component organoid model reveals field-cancerized fibroblasts as key drivers of LUAD recurrence and drug resistance

Kun Qiao,[1,7] Yanhong Huang,[2,7] Damien Chua,[3,7] Jing Qu,[4,7] Qibin Liao,[5] Guoze Wang,[2] Nguan Soon Tan,[3,6] Shumin Liao,[2] Liang Li,[2] and Guangjian Zhang[1]

[1]Department of Thoracic Surgery, the First Affiliated Hospital, Xi'an Jiaotong University, Yan Ta West Road No.277, Xi'an, Shaanxi Province 710061, China; [2]Department of Pharmacology, Joint Laboratory of Guangdong-Hong Kong Universities for Vascular Homeostasis and Diseases, School of Medicine, Southern University of Science and Technology, Shenzhen 518055, China; [3]Lee Kong Chian School of Medicine, Nanyang Technological University Singapore, 11 Mandalay Road, Singapore 308232, Singapore; [4]Department of Pathogen Biology, Shenzhen Center for Disease Control and Prevention, Shenzhen 518073, China; [5]Department of Thoracic Surgery, Shenzhen Third People's Hospital, Shenzhen 518110, China; [6]School of Biological Sciences, Nanyang Technological University Singapore, 60 Nanyang Drive, Singapore 637551, Singapore

Lung adenocarcinoma (LUAD) is a leading cause of cancer-related mortality, driven by extensive tumor heterogeneity and therapy resistance. Conventional models fail to capture the dynamic interactions between cancer cells and the tumor microenvironment (TME), limiting therapeutic advancements. Here, we present a tricomponent organoid platform integrating patient-derived lung cancer tumoroids (LCTs), normal lung organoids (LOs), and field-cancerized fibroblasts to dissect LUAD heterogeneity and treatment resistance mechanisms. This platform uniquely enables the simultaneous investigation of tumor-specific vulnerabilities, stromal contributions to drug resistance, and normal tissue toxicity. Spatial and bulk transcriptomic analyses reveal LUAD-specific gene signatures and highlight cancer-associated fibroblasts (CAFs) as key drivers of a pro-tumorigenic TME, reinforcing tumor survival and recurrence. Functional drug screening demonstrates that LCTs exhibit selective sensitivity to pemetrexed while fibroblasts remain universally resistant, underscoring stromal barriers to therapy. The inclusion of LOs allows direct assessment of drug toxicity on healthy lung tissue, bridging a critical gap in preclinical modeling. By capturing the tumor-stroma interplay with patient specificity, this organoid platform advances precision oncology, paving the way for more effective therapeutic strategies targeting both LUAD cells and the supportive microenvironment.

INTRODUCTION

Lung cancer remains the most frequently diagnosed malignancy worldwide, accounting for approximately 12.4% of all newly diagnosed cancers and projected to reach 3.8 million new cases annually by 2070.[1–3] Despite substantial advances in clinical research and therapeutic development, lung cancer continues to be the leading cause of cancer-related mortality, with an estimated 2 million deaths reported in 2022 alone.[1,2,4] This burden is driven predominantly by non-small cell lung cancer (NSCLC), which comprises >80% of all lung cancer diagnoses and is associated with a 5-year overall survival rate of <15%.

NSCLC encompasses two major histological subtypes: lung adenocarcinoma (LUAD) and lung squamous cell carcinoma (LUSC). LUAD is distinguished by pronounced phenotypic and genomic heterogeneity, resulting in extensive inter- and intratumoral variability.[5] Such heterogeneity complicates therapeutic decision-making, as tumor cells within and across patients can differ markedly in growth kinetics, invasion behavior, and molecular drivers. Clinically, this diversity translates into high relapse rates, up to 30%–50% of patients with early-stage LUAD develop metastatic recurrence following surgery resection, and nearly half ultimately relapse.[5,6]

Received 24 April 2025; accepted 26 May 2026;
https://doi.org/10.1016/j.omton.2026.201251.

[7]These authors contributed equally

Correspondence: Nguan Soon Tan, Lee Kong Chian School of Medicine, Nanyang Technological University Singapore, 11 Mandalay Road, Singapore 308232, Singapore.
E-mail: nstan@ntu.edu.sg
Correspondence: Shumin Liao, Department of Pharmacology, Joint Laboratory of Guangdong-Hong Kong Universities for Vascular Homeostasis and Diseases, School of Medicine, Southern University of Science and Technology, Shenzhen 518055, China.
E-mail: liaosm2022@sustech.edu.cn
Correspondence: Liang Li, Department of Pharmacology, Joint Laboratory of Guangdong-Hong Kong Universities for Vascular Homeostasis and Diseases, School of Medicine, Southern University of Science and Technology, Shenzhen 518055, China.
E-mail: lil@sustech.edu.cn
Correspondence: Guangjian Zhang, Department of Thoracic Surgery, the First Affiliated Hospital, Xi'an Jiaotong University, Yan Ta West Road No.277, Xi'an, Shaanxi Province 710061, China.
E-mail: michael8039@xjtu.edu.cn

A major contributor to these persistently high relapse rates is field cancerization, a process in which histologically normal-appearing tissues adjacent to tumors harbor premalignant molecular and functional alterations.[7–9] In NSCLC, accumulating evidence indicates that this phenomenon is actively shaped by cancer-associated fibroblasts (CAFs), which propagate oxidative stress and pro-tumorigenic signaling beyond the tumor core.[4,10,11] Such stromal conditioning establishes a permissive microenvironment that supports tumor progression, promotes therapy resistance, and predisposes to disease recurrence.[4] In this study, we define field-cancerized fibroblasts (FCFs) as para-tumor fibroblasts that exhibit transcriptomic and pathway signatures characteristic of CAFs, consistent with the broader concept of field cancerization whereby tumor-adjacent cells acquire pro-tumorigenic features through chronic exposure to carcinogenic and paracrine cues.

Large-scale transcriptomic analyses provide further support for the existence and biological relevance of field cancerization in NSCLC. Studies of airway epithelium have shown that tissues appearing histologically normal can display molecular signatures closely resembling those of tumors, with some genes exhibiting spatial gradients that intensify with proximity to the tumor margin.[8] Importantly, these field effects are not uniform across NSCLC subtypes: central airways tend to show more extensive damage in LUSC, whereas peripheral airways are preferentially affected in LUAD.[9] Together, these findings underscore that field cancerization is spatially structured, subtype-dependent, and likely to have distinct functional consequences in LUAD.

Despite strong evidence implicating cancerized stromal fibroblasts in therapy resistance, their molecular states and the mechanisms by which they promote LUAD relapse remain insufficiently defined. In particular, how fibroblasts within ostensibly non-malignant para-tumor tissue remodel the extracellular matrix (ECM), engage in ligand-receptor signaling, and release soluble factors to sustain tumor survival is poorly understood. Resolving these mechanisms is critical for designing therapeutic strategies that disrupt stromal support or reverse its tumor-promoting effects.

Current clinical management of early-stage LUAD typically involves surgical resection, with neoadjuvant chemotherapy or combined chemoradiation reserved for higher-risk or more advanced disease, guided by histological and molecular assessments.[12,13] However, the intrinsic heterogeneity of NSCLC, coupled with incomplete understanding of stromal contributions to recurrence and drug resistance, frequently undermines treatment durability.[14,15] These limitations highlight the need for experimental systems that can faithfully capture not only tumor-intrinsic complexity but also interactions between malignant cells and a cancerized stromal compartment.

Conventional *in vitro* and *in vivo* models, including two-dimensional cancer cell lines, primary cultures, and patient-derived xenografts (PDX), remain widely used,[16] yet each has inherent limitations. Two-dimensional cultures fail to recapitulate tumor architecture and biomechanical properties of the tumor microenvironment (TME), which are known to influence cancer cell aggressiveness and chemoresistance.[16,17] PDX models better preserve tumor heterogeneity, but their reliance on immunodeficient hosts and non-orthotopic engraftment precludes accurate modeling of immune and stromal interactions in the native lung context and requires prolonged, resource-intensive establishment.[18,19] They also require lengthy, costly development. In contrast, patient-derived lung cancer tumoroids (LCTs) retain the genetic, epigenetic, and molecular hallmarks of the parent tumors and provide a more rapid and scalable platform for therapeutic interrogation.[20–23]

Here, we integrate patient-derived LCTs, matched normal lung organoids (LOs), and para-tumor FCFs within a unified experimental framework, together with bulk and spatial transcriptomic analyses, to interrogate mechanisms of therapy resistance in LUAD. By directly comparing drug responses of tumor cells and cancerized stromal fibroblasts, and by resolving their molecular and signaling interactions, we aim to uncover underexplored drivers of relapse and chemoresistance. This tri-component platform addresses a critical gap in LUAD modeling by enabling simultaneous assessment of tumor vulnerability, stromal protection, and normal tissue tolerance, thereby providing a foundation for more precise strategies to overcome stromal-mediated therapeutic failure and disease progression.

RESULTS

Comprehensive analysis reveals LUAD heterogeneity and tumor microenvironment complexity

LUAD and LUSC are commonly grouped under the umbrella of NSCLC and often managed using similar therapeutic strategies. However, integrated transcriptomic analyses reveal that these subtypes represent biologically distinct diseases with divergent molecular architectures, underscoring the need for subtype-specific therapeutic approaches. Analysis of The Cancer Genome Atlas (TCGA) bulk sequencing (RNA-seq) data demonstrated substantial divergence between LUAD and LUSC: although 3,970 genes were shared, LUSC exhibited 4,533 subtype-specific genes, whereas LUAD displayed 2,232 unique genes (Figure 1A). These differences highlight the necessity of precision medicine strategies tailored to the LUAD-specific genomic landscape.

Further interrogation of LUAD-specific transcriptional signatures across TCGA and in-house datasets uncovered pronounced inter-patient heterogeneity, consistent with the diverse histological patterns observed clinically (Figure 1B). This variability was partly attributable to differential infiltration by stromal and immune populations, reflecting the complexity of the LUAD TME. Despite this heterogeneity, LUAD samples consistently maintained a distinct molecular identity when compared with normal lung tissue (Figure 1C). Gene ontology analyses revealed coordinated upregulation of immune-related and ECM remodeling pathways, including collagen degradation and TGFβ1 signaling, alongside downregulation of epithelial proliferation and angiogenesis pathways (Figures 1D and 1E). Collectively, these data indicate a significant

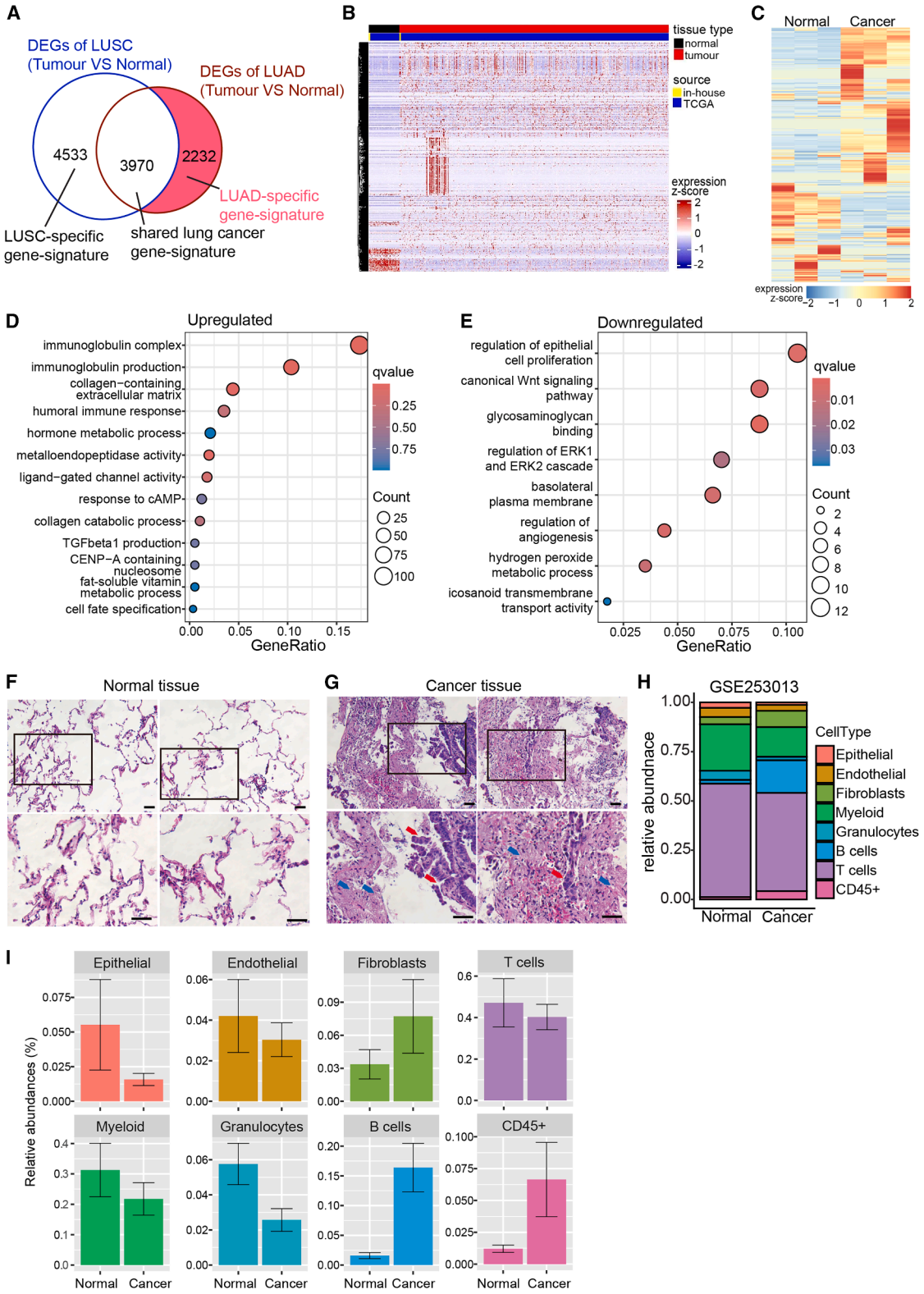

(legend on next page)

remodeling of lung architecture in LUAD. Together, these transcriptional programs indicate extensive remodeling of lung tissue architecture in LUAD.

Histopathological examination corroborated these molecular findings, revealing marked alterations in tissue organization, including glandular and papillary structures, invasive growth patterns, and nuclear atypia (Figures 1F and 1G). Collectively, these features reflect a tumor ecosystem characterized by both malignant epithelial transformation and substantial stromal reprogramming.

Single-cell RNA sequencing (scRNA-seq) further resolved the cellular composition of the LUAD TME, identifying eight major populations: epithelial cells, endothelial cells, fibroblasts, myeloid cells, granulocytes, B cells, T cells, and $CD45^+$ immune cells (Figure 1H). Compared with normal lung tissue, LUAD exhibited a reduced epithelial fraction accompanied by enrichment of stromal and immune compartments, with CAFs emerging as a particularly prominent population (Figure 1I). This cellular composition aligns with histological observations, in which CAFs were abundant and exhibited spindle-shaped, disorganized morphologies throughout LUAD specimens. Given their established roles in ECM remodeling, these CAFs likely contribute directly to tumor invasion and progression, positioning them as major drivers of LUAD heterogeneity.

Taken together, these integrated bulk transcriptomic, histological, and single-cell analyses underscore the multifaceted nature of LUAD and identify CAFs as central components of a remodeled, resilient TME. These findings suggest that stromal fibroblasts are not passive bystanders but active determinants of tumor plasticity, therapeutic resistance, and disease recurrence.

CAFs as key mediators of tumor-stroma interplay in LUAD

To define how distinct cellular compartments coordinate to sustain LUAD growth and resilience, we next applied spatial transcriptomics at single-cell resolution. Seven major tumor-associated cell clusters were identified, including adenocarcinoma cells, B cells, endothelial cells, fibroblasts, macrophages, mast cells, and T cells (Figure S1A). Notably, the patient-derived dataset displayed a unique TME composition, with adenocarcinoma cells accounting for 8.37% of cells, fibroblasts for 17.7%, and endothelial cells for 10.7%. In contrast, B cells were markedly enriched (37.8%), while T cells were comparatively underrepresented (6.49%), diverging from patterns observed in the independent GSE253013 cohort and highlighting substantial inter-patient heterogeneity (Figures 2A and 2B).

Cell-cell communication analysis using CellChat revealed a highly interconnected signaling network within the LUAD TME. Endothelial cells emerged as dominant signal senders, followed closely by fibroblasts and macrophages, whereas adenocarcinoma cells were the principal signal recipients (Figure 2C). Among stromal populations, fibroblasts exerted a particularly strong influence on adenocarcinoma cells, surpassing even endothelial cells in their predicted signaling impact (Figures 2B and 2C). Spatial mapping further demonstrated that fibroblasts were preferentially co-localized with adenocarcinoma cells, exhibiting a higher fibroblast-to-tumor cell ratio (2.11) compared with endothelial cells (1.28) (Figures 2D–2F).

Importantly, spatial and signaling analyses revealed evidence of ERBB2-associated amplification of CAF activity, suggesting that oncogenic ERBB2 signaling may potentiate tumor-stroma crosstalk. This observation reinforces the concept that CAFs function as a central signaling nexus within the LUAD microenvironment, integrating oncogenic cues to reinforce tumor survival and progression.

Collectively, these data position CAFs as key orchestrators of tumor-stroma communication in LUAD, driving ligand-receptor interactions that expand and stabilize a tumor-supportive niche. Targeting CAF-mediated signaling pathways therefore represents a promising strategy to disrupt stromal support, overcome therapy resistance, and mitigate disease recurrence in this heterogeneous malignancy.

Patient-specific tumoroid-CAF platform reveals stromal drug resistance in LUAD

Building on our observations that LUAD heterogeneity is strongly shaped by CAFs and adjacent field-cancerized tissues, we developed a three-dimensional (3D) culture platform designed to recapitulate these stromal interactions in a patient-specific manner. This tri-component system integrates (1) patient-derived LCTs, (2) normal

Figure 1. Integrated transcriptomic, histological, and single-cell analysis reveals LUAD-specific heterogeneity and stromal enrichment

(A) Venn diagram showing differentially expressed genes (DEGs) identified from tumor versus normal comparisons in lung adenocarcinoma (LUAD) and lung squamous cell carcinoma (LUSC). Shared lung cancer gene signatures and subtype-specific DEGs unique to LUAD or LUSC are indicated. (B and C) Heatmaps of LUAD-specific gene signatures comparing tumor and normal lung tissue. (B) Integrated analysis of TCGA and in-house datasets demonstrates consistent LUAD-associated expression patterns across cohorts. (C) An independent in-house patient dataset confirms these LUAD-specific transcriptional signatures. Gene expression is shown as z-scores, with red indicating upregulation and blue indicating downregulation. (D and E) Gene Ontology (GO) enrichment analysis of LUAD tumor DEGs. (D) Upregulated pathways are enriched for immune responses and extracellular matrix (ECM) remodeling processes, including collagen metabolism and TGF-β signaling. (E) Downregulated pathways include epithelial cell proliferation, canonical Wnt signaling, and angiogenesis-related processes. Dot size reflects the number of genes per pathway, and color indicates statistical significance (*q* value). (F and G) Representative H&E-stained sections of (F) normal lung tissue and (G) LUAD tissue. Tumor sections show marked architectural disruption and stromal expansion. Red arrows indicate cancerous regions, while blue arrows highlight cancer-associated fibroblasts (CAFs). Scale bars, 50 μm. (H) Stacked bar plot showing relative proportions of major cell types derived from the single-cell RNA-seq dataset GSE253013, comparing normal lung and LUAD tissues. Cell types include epithelial, endothelial, fibroblast, myeloid, granulocyte, B cell, T cell, and $CD45^+$ immune populations. (I) Boxplots summarizing relative abundances (%) of individual cell populations in normal versus LUAD tissues from GSE253013, highlighting depletion of epithelial cells and enrichment of stromal and immune compartments, including fibroblasts/CAFs, in LUAD.

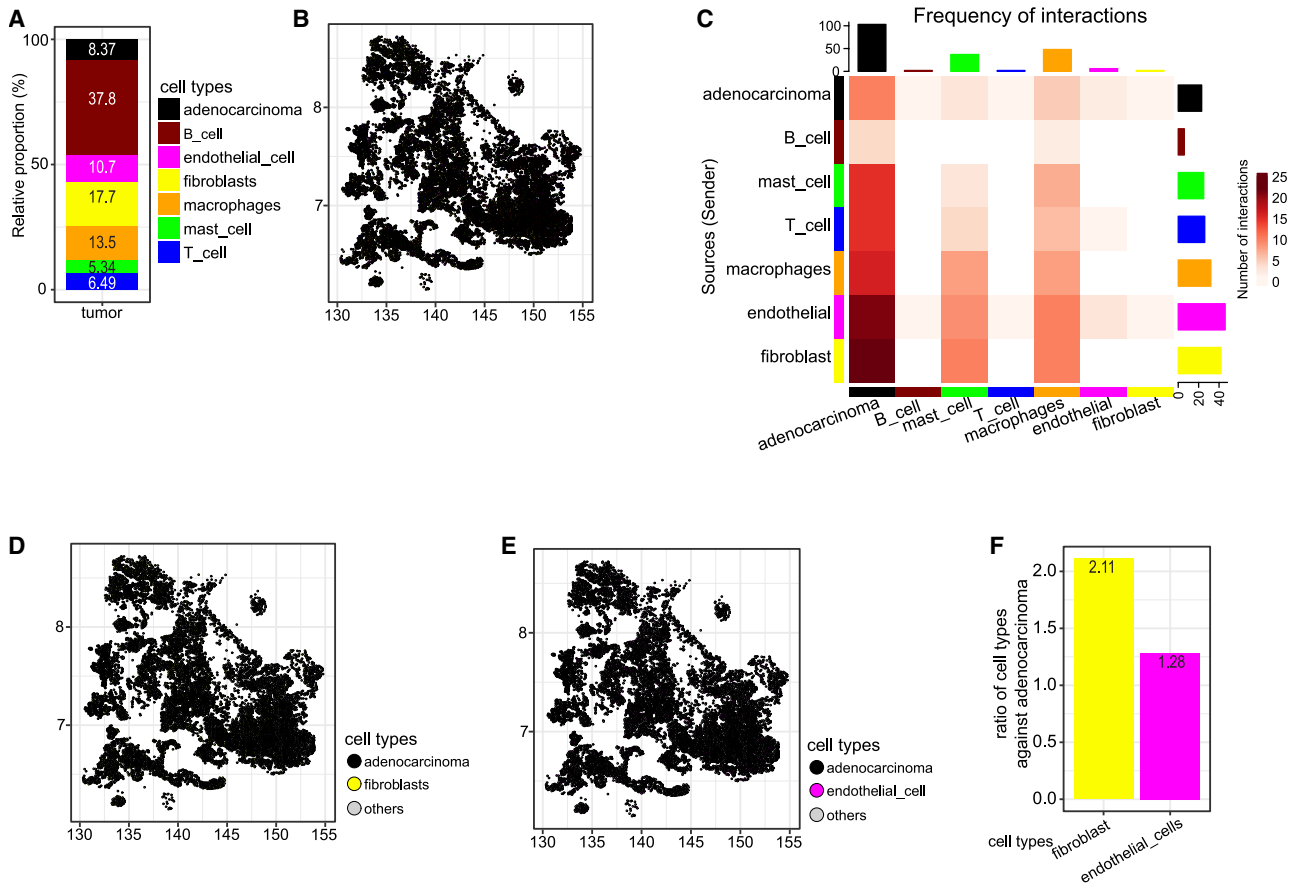

Figure 2. Spatial transcriptomic analysis identifies fibroblasts as dominant mediators of tumor-stroma interactions in LUAD

(A) Stacked bar plot showing the relative proportions of major cell types identified by spatial transcriptomics in LUAD tumor tissue, including adenocarcinoma cells, fibroblasts, endothelial cells, and immune populations. (B) Two-dimensional embedding of spatial transcriptomic single cells colored by annotated cell type, illustrating the spatial organization and intermixing of tumor and stromal compartments within the LUAD tissue section. (C) Heatmap of spatial proximity-based cell-cell interaction frequencies, showing enrichment or depletion of interactions between sender (rows) and receiver (columns) cell types. Interaction enrichment was calculated by comparing observed spatial adjacency to expected frequencies derived from 2,000 randomized spatial network simulations. Fibroblasts and endothelial cells emerge as prominent signal-sending populations toward adenocarcinoma cells. (D and E) Spatial maps showing the distribution of adenocarcinoma cells in relation to (D) fibroblasts and (E) endothelial cells, highlighting preferential co-localization of fibroblasts with tumor cells compared with endothelial cells. (F) Quantification of stromal cell enrichment relative to adenocarcinoma cells, expressed as ratios of fibroblasts and endothelial cells to tumor cells. Fibroblasts display a higher relative abundance (ratio = 2.11) than endothelial cells (ratio = 1.28), consistent with their dominant spatial association with tumor regions.

LOs, and (3) fibroblasts isolated from para-tumor field-cancerized tissues.

We established a clinically relevant workflow that enables the parallel generation of LCTs and LOs from surgical specimens within a two-week window between tumor resection and initiation of consolidation chemotherapy (Figure 3A). In culture, LCTs formed dense spheroidal structures with diameters of 50–150 μm, closely resembling the compact architecture of primary LUAD tumors, whereas LOs formed larger, vesicular structures up to 200 μm in diameter that retained morphological features of normal lung epithelium (Figure 3B). This configuration allowed direct, compartment-resolved assessment of drug responses across tumor, stromal, and normal tissue components within a single experimental framework.

Using this platform, we evaluated the effects of pemetrexed, cisplatin, and toripalimab on LCTs, cancerized fibroblasts, and LOs. LCTs exhibited marked sensitivity to pemetrexed, with viability reduced to approximately 20% at 1.0 ng/mL and below 5% at 5.0 ng/mL. In contrast, cisplatin and toripalimab produced minimal effects on LCT viability, which remained above 80% across tested concentrations (Figure 3C). Strikingly, fibroblasts isolated from para-tumor tissues were uniformly resistant to all three agents, maintaining nearly 100% viability under all treatment conditions (Figure 3D).

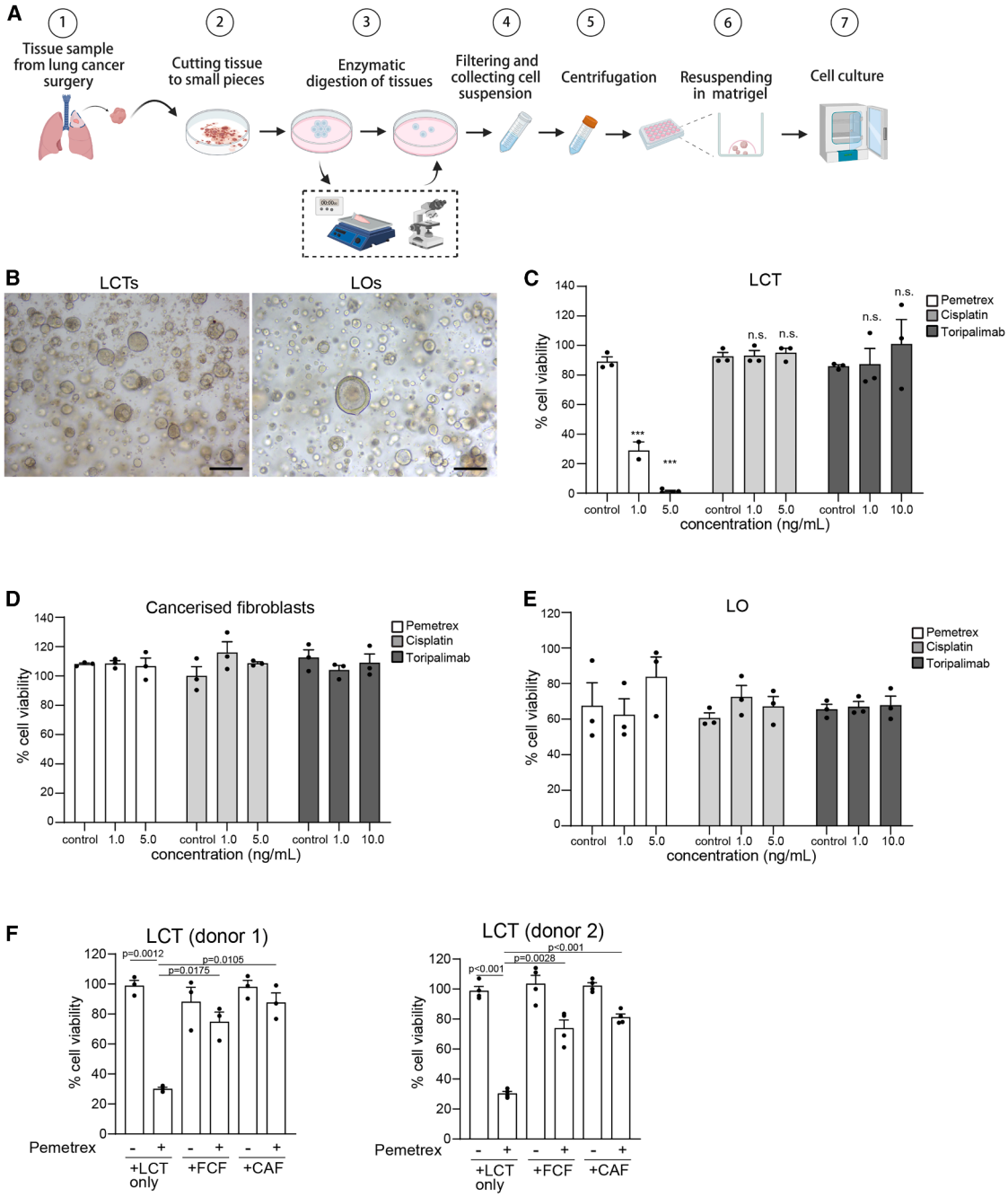

Figure 3. Stromal fibroblasts are intrinsically drug resistant and functionally confer pemetrexed resistance to LUAD tumoroids

(A) Schematic workflow for generating patient-derived lung cancer tumoroids (LCTs) from surgical specimens. Steps include (1) collection of fresh lung cancer tissue, (2) mechanical dissociation into small fragments, (3) enzymatic digestion under controlled conditions, (4) filtration and cell suspension collection, (5) centrifugation to isolate viable cells, (6) resuspension in Matrigel, and (7) 3D culture maintenance under optimized growth conditions. This process preserves the characteristics of the original tumor tissue. (B) Representative phase-contrast images of LCTs and matched normal lung organoids (LOs). LCTs form dense, multicellular spheroids, whereas LOs adopt vesicular morphologies characteristic of normal lung epithelium. Patient-derived fibroblasts exhibit elongated, spindle-shaped morphology. Scale bars, 200 μm. (C–E) Drug sensitivity profiles of (C) LCTs, (D) cancerized fibroblasts, and (E) LOs following treatment with pemetrexed (1.0 and 5.0 ng/mL), cisplatin (1.0 and 5.0 ng/mL), or toripalimab (1.0 and 10.0 ng/mL). LCTs show pronounced sensitivity to pemetrexed (***$p < 0.001$), while cisplatin and toripalimab have minimal effects. Cancerized fibroblasts are uniformly resistant to all tested agents, whereas LOs display modest baseline viability with no significant additional drug-induced cytotoxicity. Cell viability is expressed as a percentage of untreated controls (mean ± SD; $n = 3$ independent experiments). (F) Co-culture assays demonstrating stromal-mediated chemoresistance. LCTs from two independent

(legend continued on next page)

Normal LOs displayed modest baseline viability (60%–70%) but were similarly unaffected by drug exposure (Figure 3E).

To determine whether fibroblast drug resistance translated into functional protection of tumor cells, we performed co-culture experiments in which LCTs were cultured with either FCFs or CAFs and treated with pemetrexed. In both donor 1 and donor 2, pemetrexed treatment alone reduced LCT viability to approximately 30%. However, co-culture with FCFs increased LCT viability to ∼75% and ∼70%, respectively, while CAF co-culture further enhanced viability to >80% in donor 1 and ∼80% in donor 2 (Figure 3F). These findings indicate that fibroblasts from both tumor and para-tumor regions are associated with increased tumor cell survival under chemotherapy.

Collectively, these results confirm pemetrexed efficacy against LUAD tumor cells while revealing a critical therapeutic gap: stromal fibroblasts that are intrinsically drug resistant and capable of shielding tumor cells from chemotherapy. Without strategies to overcome this stromal barrier, tumor-directed therapies alone may be insufficient to achieve durable remission.

Field cancerization in para-tumor tissue is associated with a transformed CAF-like fibroblast phenotype

Motivated by the pronounced drug resistance of fibroblasts derived from tumor-adjacent tissues, we next examined whether these cells exhibit molecular features consistent with field cancerization. In culture, para-tumor fibroblasts displayed the spindle-shaped morphology typical of CAFs (Figure 4A). Immunofluorescence staining for vimentin and F-actin (phalloidin) confirmed their fibroblast identity (Figure 4B); however, these canonical markers did not distinguish them from fibroblasts derived from non-malignant tissue, necessitating deeper molecular characterization.

Bulk RNA-seq revealed a marked shift in the transcriptomic profiles of para-tumor fibroblasts toward a cancer-associated state (Figure 4C). Gene enrichment analyses demonstrated significant upregulation of pathways involved in collagen metabolism and ECM remodeling, hallmark features of CAF function (Figure 4D). These data indicate that fibroblasts within histologically normal adjacent tissue can undergo functional reprogramming into a tumor-supportive state that is not apparent at the level of standard fibroblast markers.

In parallel, gene set enrichment analysis (GSEA) confirmed that patient-derived LCTs recapitulated core LUAD molecular programs, including enhanced cell-cycle activity (NES = 1.85), elevated reactive oxygen species (ROS) response pathways (NES = 2.30), and altered organellar functions such as ciliogenesis (NES = 1.86) (adjusted $p < 0.05$ for all; Figure 4E).

To define how cancerized fibroblasts communicate with tumor cells, we performed ligand-receptor interaction analysis using the CellChat R package. This analysis revealed predominantly fibroblast-driven signaling toward adenocarcinoma cells. Specifically, fibroblast-derived ligands including COL1A1 and FN1 engaged tumor-cell receptors ITGA3-ITGB1 and CD44 (Figure 4F), whereas endothelial cells primarily communicated with tumor cells through APP-CD74 interactions (Figure S1B). These results identify fibroblasts as major signaling contributors within the LUAD microenvironment.

To investigate the functional relevance of candidate receptor pathways, we performed siRNA-mediated knockdown of CD44 or ITGA3/ITGB1 in LCT-CAF co-cultures. In donor 1, CD44 knockdown significantly reduced LCT viability under pemetrexed from ∼86.8% to ∼47.3%, while ITGA3/ITGB1 knockdown resulted in a more modest but significant reduction to ∼67.2%.

In donor 2, CAF co-culture elevated LCT viability from 29.3% to only 54.6% under pemetrexed—a markedly attenuated protective effect relative to donor 1, indicating that tumor-intrinsic resistance mechanisms beyond the CAF-tumor axis may contribute to the overall chemoresistance landscape in this donor. Nevertheless, CD44 knockdown produced a significant reduction in viability to ∼43.8%, confirming a consistent, albeit donor scaled, contribution of CD44 to stromal chemoprotection. In contrast, ITGA3/ITGB1 knockdown had no appreciable effect in donor 2 (Figure 4G), suggesting that integrin-mediated pathways are not uniformly engaged across patients. Taken together, these findings implicate CD44 as a reproducible mediator of CAF-conferred resistance while highlighting the patient-specific nature of integrin involvement, consistent with heterogeneous and personalized TME chemoresistance programs. siRNA treatment alone did not affect baseline LCT viability in either donor, confirming that observed effects were contingent on pharmacological and cytotoxic challenge.

Taken together, these results support a previously underappreciated FCF state in para-tumor lung tissue and a model in which stromal fibroblasts contribute to a chemoprotective niche that attenuates pemetrexed efficacy in LUAD. While the magnitude and mechanistic drivers of this effect vary between donors, the overall phenomenon remains consistent, underscoring the robustness of stromal-mediated protection. Importantly, the observed inter-donor variability highlights that these interactions are not governed by a single universal pathway but instead reflect patient-specific dependencies. This

LUAD donors were cultured alone or co-cultured with matched field-cancerized fibroblasts (FCFs) or cancer-associated fibroblasts (CAFs) and treated with vehicle or pemetrexed. Co-culture with either FCFs or CAFs significantly attenuated pemetrexed-induced cytotoxicity in LCTs, restoring tumor cell viability relative to LCT-only cultures. Data are shown as mean ± SEM (n = 3–5 biological replicates); dots represent individual replicates. p values reported in respective comparisons were calculated using unpaired two-tailed t tests.

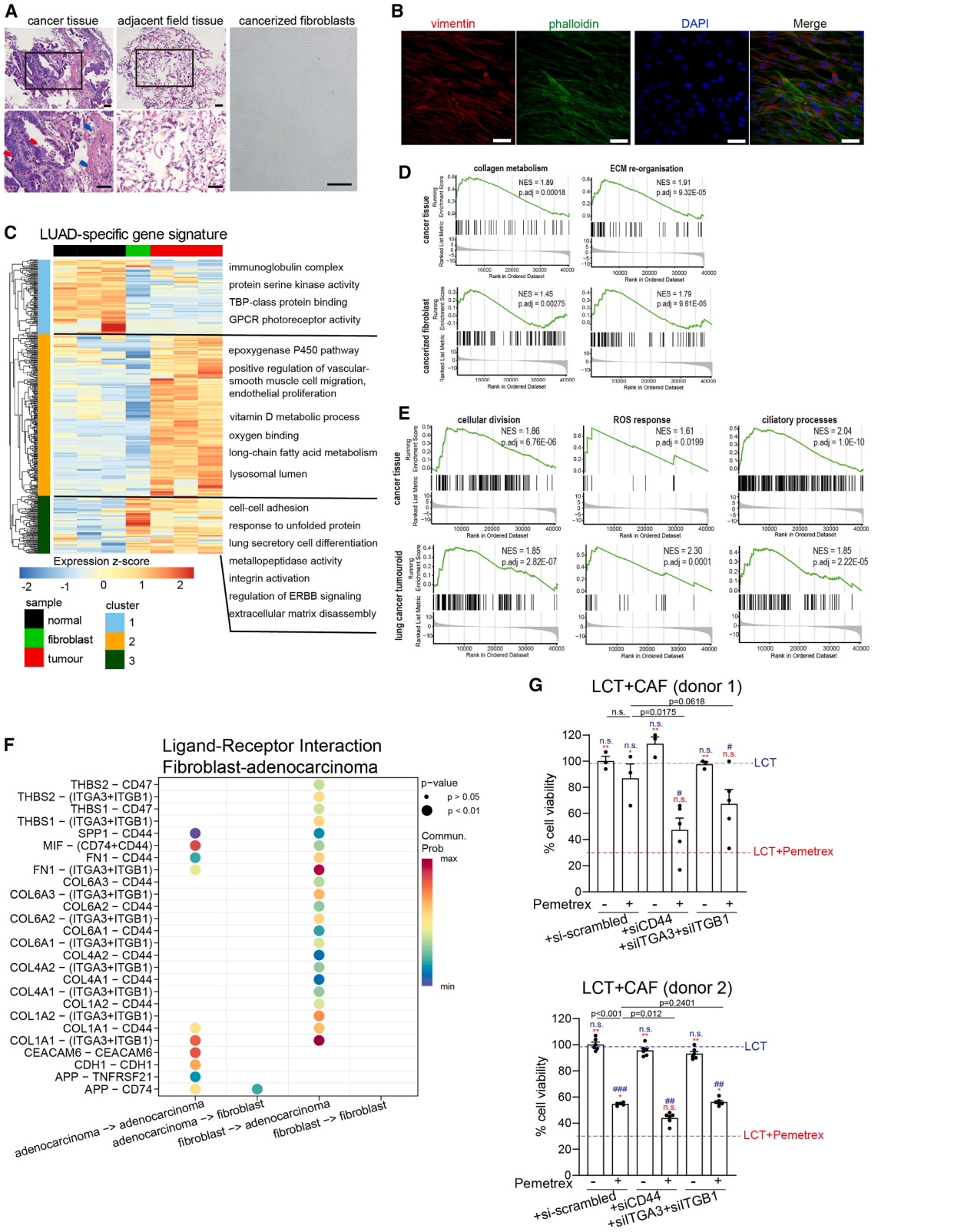

(legend on next page)

reinforces the need for comprehensive tumor and microenvironmental profiling to accurately resolve the dominant resistance mechanisms in each context. In this light, our findings not only validate the functional importance of stromal-tumor interactions but also emphasize that effective therapeutic strategies will likely require stratified, precision-based approaches rather than uniform targeting of a single pathway. By enabling integrated analysis of tumor, stromal, and normal compartments, the tri-component organoid platform provides a foundation for mechanistic dissection of stromal-mediated resistance and the development of personalized strategies to disrupt the tumor-stroma niche.

DISCUSSION

In this study, we established a tri-component organoid system that integrates patient-derived LCTs, matched normal LOs, and fibroblasts isolated from peri-tumoral tissue. Unlike conventional tumor-centric models, this platform preserves reciprocal interactions among malignant epithelial cells, stromal fibroblasts, and healthy lung tissue within a unified experimental framework. By anchoring the model to deep phenotyping and spatial transcriptomic analyses of the originating patient tumors, we capture both intra- and inter-tumoral heterogeneity that is frequently obscured in reductionist systems and that likely underlies the limited durability of standardized therapies. As such, the tri-component platform provides a physiologically relevant context for dissecting tumor-stroma interactions and for evaluating patient-specific therapeutic vulnerabilities.

A central finding of this work is that fibroblasts derived from histologically normal para-tumoral tissue exhibit pervasive drug resistance and exert a dominant influence on tumor cell survival under chemotherapy stress. Although these cells express canonical stromal markers such as vimentin and F-actin, transcriptional profiling reveals a reprogrammed molecular state consistent with field cancerization. This observation supports a model in which carcinogen exposure and chronic paracrine signaling extend beyond the tumor core to establish a pre-conditioned stromal niche that actively sustains tumor persistence and recurrence. The close proximity of these CAFs to cancer cells suggests they not only promote tumor survival but also maintain therapeutic resistance by establishing a protective niche. This observation aligns with growing evidence that precancerous lesions and primary tumors often share transcriptomic profiles, positioning CAFs as central mediators of LUAD heterogeneity and recurrence. Importantly, this stromal drug resistance was conserved across all tested therapies, whereas normal LOs displayed limited sensitivity to pemetrexed, underscoring both the selectivity of tumor-directed effects and the relative safety of this agent in non-malignant tissue. Together with the observed association between cisplatin resistance and absent ERCC1 expression,[24] and the modest response to toripalimab in line with known limitations of PD-1 blockade in EGFR/ALK-altered NSCLC,[25] these findings emphasize that therapeutic failure in LUAD cannot be fully explained by tumor-intrinsic mechanisms alone.

Conceptually, our data reinforce the view that FCFs function as active regulators of the TME rather than passive bystanders. Similar to malignant epithelial cells, these fibroblasts appear to undergo stable molecular reprogramming, acquiring pro-survival and matrix-remodeling capabilities that reinforce tumor plasticity and therapeutic resistance. The inability of standard fibroblast markers to distinguish these cancerized fibroblasts from ostensibly normal counterparts highlights a critical diagnostic blind spot and underscores the need for molecularly informed stratification of stromal states. By enabling simultaneous interrogation of malignant, stromal, and healthy compartments, the tri-component organoid model directly addresses this gap and allows functional dissection of stromal contributions to drug response.

Mechanistically, the identification of CD44 and ITGA3-ITGB1 as tumor-cell receptors mediating CAF-driven protection provides a tractable entry point for therapeutic intervention. The ability to partially restore chemosensitivity through genetic perturbation of these signaling axes demonstrates that stromal-mediated resistance

Figure 4. Field-cancerized fibroblasts exhibit CAF-like molecular programs and mediate tumor chemoresistance through defined ligand-receptor signaling axes

(A) Representative H&E-stained sections of LUAD tumor tissue, adjacent field tissue, and phase-contrast images of cultured cancerized fibroblasts. Tumor tissue displays disrupted alveolar architecture with expanded stromal regions (red arrows indicate tumor areas; blue arrows indicate cancer-associated fibroblasts). Adjacent field tissue lacks normal alveolar organization. Cultured fibroblasts show elongated spindle-shaped morphology. Scale bars, 50 μm. (B) Immunofluorescence staining of field-cancerized fibroblasts for vimentin (red), F-actin cytoskeleton (phalloidin; green), and nuclei (DAPI; blue), confirming mesenchymal fibroblast identity. Scale bars, 50 μm. (C) Heatmap of LUAD-specific gene signatures across normal lung tissue, LUAD tumor tissue, and cultured patient-derived fibroblasts. Expression values are shown as z-scores. Field-cancerized fibroblasts cluster more closely with tumor tissue than with normal lung tissue, indicating acquisition of tumor-associated transcriptional programs. (D) Gene set enrichment analysis (GSEA) comparing LUAD tumor tissue and cancerized fibroblasts, revealing significant enrichment of pathways related to collagen metabolism and extracellular matrix (ECM) reorganization in fibroblasts. (E) GSEA of LUAD tumor tissue and patient-derived lung cancer tumoroids, demonstrating enrichment of tumor-associated pathways including cellular division, reactive oxygen species (ROS) response, and ciliatory processes. (F) Ligand-receptor interaction analysis (CellChat) depicting dominant fibroblast-to-adenocarcinoma signaling. Dot size represents statistical significance (*p* value), and color denotes communication probability. Prominent interactions include ECM-derived ligands (e.g., COL1A1, COL1A2, FN1) engaging tumor-cell receptors ITGA3–ITGB1 and CD44. Endothelial-derived interactions are shown for comparison. (G) Functional validation of stromal-mediated chemoresistance. Lung cancer tumoroids (LCTs) from two independent donors were co-cultured with CAFs and transfected with control siRNA (si-scramble), siRNA targeting tumor-cell CD44, or combined ITGA3/ITGB1, followed by vehicle or pemetrexed treatment. Knockdown of tumor-cell receptors partially restored pemetrexed sensitivity in CAF-protected LCTs, with donor-specific differences in receptor dependence. Cell viability is normalized to untreated LCT-only controls (blue dashed line); red dashed line indicates LCT + pemetrexed baseline. Bars represent mean ± SEM ($n = 3–5$ biological replicates); dots denote individual replicates. *p* values were calculated using unpaired two-tailed *t* tests.

is not immutable and can be disrupted at defined molecular nodes. Notably, the relative contribution of individual receptors differed between patients, underscoring the personalized nature of tumor-stroma dependencies and reinforcing the need for patient-specific modeling approaches when considering stromal co-targeting strategies.

Several limitations of this study warrant consideration. First, although the 3D co-culture system recapitulates key aspects of the TME more faithfully than monolayer cultures, *in vivo* validation will be necessary to define how FCFs influence tumor progression, immune interactions, and metastatic dissemination in an intact organism. Second, while we demonstrate reproducible stromal drug resistance across two independent stage IIIA LUAD donors and anchor our findings to large transcriptomic cohorts, broader validation across additional patients, molecular subtypes, and disease stages will be required to fully assess generalizability. Third, ethical and practical constraints preclude routine acquisition of healthy lung fibroblasts for direct comparison, however, benchmarking against population-scale single-cell datasets provides complementary evidence that the fibroblast states described here align with CAF-like programs observed across LUAD cohorts. Fourth, the present analyses are confined to a single clinical stage and extending this framework to earlier and later disease stages will be essential to determine whether stromal drug resistance is conserved or evolves during disease progression. Finally, the limited donor cohort ($n = 2$) constrains broad causal generalization, and conclusions regarding CD44 and integrin-associated pathways in pemetrexed resistance should be interpreted within the proof-of-concept scope of this study. The donor-specific differences in drug sensitivity and perturbation response are nonetheless mechanistically informative: they indicate that these pathways operate in a context-dependent manner and are not components of a uniform resistance mechanism but rather reflect patient-specific configurations of stromal-tumor signaling. This heterogeneity is consistent with emerging evidence that resistance programs are patient-specific in their architecture and supports the utility of our experimental platform as a system for resolving such variation at pathway resolution. A further technical consideration is that siRNA-mediated knockdown achieving 40%–50% transcript reduction may not produce equivalent protein depletion, particularly for membrane-associated targets with high baseline abundance or turnover. This represents a conservative perturbation, and the functional signals identified in donor 1 under these conditions likely underestimate the full contribution of these pathways. The absence of a detectable phenotype in donor 2 following integrin knockdown may reflect a combination of incomplete protein depletion and genuine inter-donor biological divergence and should not be interpreted as a negative result. Future studies incorporating larger donor cohorts and orthogonal perturbation strategies will be required to establish causal generalizability and to define the conditions under which CD44 and integrin-associated pathways constitute tractable therapeutic vulnerabilities in stromal-mediated chemoresistance.

Despite these limitations, our findings prompt a re-evaluation of current therapeutic paradigms in LUAD. Effective treatment strategies must move beyond tumor-centric approaches to address the reciprocal tumor-stroma crosstalk that stabilizes drug resistance and fuels recurrence. By explicitly incorporating FCFs into patient-derived models, the tri-component organoid system provides a practical and scalable platform for testing combination or sequential strategies that simultaneously target malignant cells and their supportive stromal niche.

Conclusions

In summary, this study demonstrates that LUAD-associated transformation extends beyond malignant epithelial cells into adjacent stromal fibroblasts, generating field-cancerized populations that are intrinsically drug resistant and capable of protecting tumor cells from chemotherapy. The failure of conventional fibroblast markers to capture this altered state highlights a fundamental limitation in current diagnostic and modeling approaches. By integrating patient-derived tumor cells, normal LOs, and FCFs, we establish a high-fidelity *in vitro* platform that preserves the functional complexity of the LUAD microenvironment. This system not only clarifies the role of cancerized stroma in therapeutic failure but also enables mechanistic interrogation and patient-specific targeting of stromal pathways. Targeting these FCFs and their signaling interfaces with tumor cells represents a promising avenue for improving treatment durability and reducing recurrence in LUAD.

MATERIALS AND METHODS

Patient samples

Patients with advanced stage III LUAD were recruited for this study prior to surgical resection at Shenzhen Third People's Hospital ($n = 2$). None of the patients had a history of lung infection or other active infectious diseases at the time of surgery. Resected lung tissues were categorized based on pathological assessment into tumor tissue (malignant regions) and para-tumor tissue (adjacent, histologically non-malignant regions). All samples used in this study were surplus to routine clinical diagnostic procedures, including pathological evaluation, and would otherwise have been discarded. The study was conducted in accordance with the Declaration of Helsinki and was approved by the Institutional Review Board of Shenzhen Third People's Hospital (approval no. 2021-030-08). Written informed consent was obtained from all participants prior to sample collection.

Spatial transcriptomics

Formalin-fixed paraffin-embedded (FFPE) blocks were sectioned at 5 μm thickness and incubated at 60°C overnight to melt the paraffin. Spatial transcriptomics was performed by YuceBio, Inc. (Shenzhen, China). The procedure involved target retrieval and protease digestion before the application of fiducials. Post-fixing of tissue was performed, followed by blocking and overnight hybridization. Nuclear staining was applied before incubation with the segmentation mix. The flow cell assembly tool was used to load flow cells, reagents, and sample cells. Samples were then sequenced using the CosMx Spatial Molecular Imager (NanoString Technologies, Inc., USA). Bioinformatics analysis using *Seurat* R package is used to identify cell clusters and annotate their identities and interrogate

transcriptomic profiles of the tissue compartments.[26] Subsequently, colocalization and ligand-receptor analyses were performed using *CellChat* R package.[27]

Single-cell dissociation of patient samples

Surgically resected tissue samples (~1 cm^3) were transported on ice to the laboratory within 1 h of removal, in cold DMEM medium. The samples were washed three times with cold Dulbecco's phosphate-buffered saline (DPBS). Tissue was incubated with 0.001% DNase (Sigma-Aldrich, St. Louis, MO, USA), 1 mg/mL collagenase/dispase (Roche, Basel, Switzerland), and 100 U/mL penicillin-streptomycin in DMEM/F12 medium at 37°C for 20 min with intermittent agitation. Following enzymatic digestion, the cell suspensions were resuspended by pipetting. Cells were centrifuged at 350 × *g* for 5 min, and the pellet was resuspended in Matrigel (Corning, NY). After a 20-min incubation at 37°C, pre-warmed organoid medium (DMEM/F12 supplemented with noggin, R-spondin, B27 (Invitrogen), nicotinamide, N-acetylcysteine, FGF7, FGF10, A83-1, SB202190, Y27632, HEPES, and GlutaMAX) was added. The medium was refreshed every 3 days. Fibroblasts were cultured from approximately 5 mm^3 lung tissue in DMEM with 10% FBS.

Culture and passaging of LCTs, LOs, and fibroblasts

For passaging, a solidified Matrigel drop containing organoids was harvested using cold DPBS and centrifuged at 350×g for 5 min at 4°C. Organoids were resuspended in 1 mL of Tryple Express (Gibco) and incubated at 37°C for 5 min to dissociate. Following this, 10 mL of DMEM/F12 was added, and the samples were centrifuged at 350 × *g* for 5 min. The pellets were washed with DPBS and centrifuged again at 350 × *g* for 5 min. The pellets were then resuspended in Matrigel and reseeded at a 1:3–1:4 ratio to allow new organoid formation. For fibroblasts, cells were passaged by digestion with 0.25% trypsin for 3 min, followed by neutralization with DMEM containing 10% FBS. Fibroblasts were cultured in DMEM with 10% FBS.

RNA-seq

RNA-seq was conducted by Chi Biotech (Shenzhen, China). RNA was extracted and subjected to quality control before library construction. Quantification was performed using a Qubit 2.0 Fluorometer, and library insert size was assessed with an Agilent 4200 TapeStation. Sequencing was carried out on the NovaSeq 6000 platform with a PE150 strategy. Sequence alignment was performed using STAR software against HUMAN GENCODE 34 GRCh37 (11.2019). Quantitative analysis was carried out with FeatureCounts, and gene expression was quantified as TPM (transcripts per kilobase of exon model per million mapped reads). Differentially expressed genes (DEGs) were identified using criteria of $|\log2FC| > 1$ and $p < 0.05$. DEGs were further analyzed for functional annotation and gene set enrichments.[28]

Drug screening trials

Patient-derived LCTs were cultured for approximately 14 days until reaching a diameter of ~200 μm, after which they were transferred to 384-well plates and allowed to acclimatize for 3 days prior to treatment. Fibroblasts were seeded into 384-well plates upon reaching ~80% confluency in T25 flasks.

Drug screening was performed using standard NSCLC therapeutics, including pemetrexed, cisplatin, and toripalimab. All compounds were purchased from MedChemExpress (MCE; New Jersey, USA) and administered at five concentrations for a treatment duration of 3 days. Cell viability of tumoroids was quantified using the CellTiter-Glo 3D Luminescence Cell Viability Assay (Promega, USA) according to the manufacturer's protocol. Briefly, CellTiter-Glo 3D reagent was added to cultures at a 1:1 (v/v) ratio, plates were shaken at room temperature for 5 min, followed by incubation at room temperature for an additional 25 min before luminescence measurement.

For receptor knockdown experiments, siRNAs targeting CD44, ITGA3, or ITGB1 (TsingKe) were transfected into LCTs using Lipofectamine 3000 (Invitrogen; cat. #L3000015) at a final siRNA concentration of 500 nM. Transfection was performed for 24 h prior to treatment with pemetrexed (50 ng/mL). Knockdown efficiency for each target exceeded 50%, as validated by RT-PCR analysis (Figure S2).

Statistical analysis

Drug response curves were plotted and IC50 values calculated using GraphPad Prism 9.5 (GraphPad Software, La Jolla, CA, USA). Statistical significance was defined as $p < 0.05$.

DATA AND CODE AVAILABILITY

High-throughput sequencing raw and processed data can be found in the GEO databases (GSE287471 and GSE287472). The programmatic scripts used for bioinformatic analysis are available at Github (https://github.com/chua-damien/LUAD-tumoroids/).

ACKNOWLEDGMENTS

The work was supported by the National Key Research and Development Program of China (2022YFC2304400, 2022YFC2304401), Sanming Project of Medicine in Shenzhen (SZSM202311034), the Natural Science Foundation of Guangdong Province of China (2021A1515010004), Special Funds for Strategic Emerging Industry of Shenzhen (F-2022-Z99-502266), SUSTech Starting-up Research Grant (Y01416133), and the Shenzhen Science and Technology Program (JCYJ20190809143601759, JCYJ20210324130601005, RCBS20221008093104016). D.C. is a recipient of the Nanyang Presidential Graduate Scholarship and SUSTech Fellowship. Schematic figures were generated using Biorender.com.

AUTHOR CONTRIBUTIONS

K.Q., Y.H., S.L., L.L., and G.Z. contributed to the study design. K.Q., Y.H., G.W., Q.L., and G.Z. contributed to the collection of clinical samples and clinical data. K.Q., Y.H., G.W., and S.L. contributed to the experiments. K.Q., Y.H., D.C., S.L., J.Q., L.L., and G.Z. contributed to the data analysis. K.Q., Y.H., D.C., N.S.T., S.L., L.L., and G.Z. contributed to the manuscript preparation. All the authors have read, edited, and approved the manuscript.

DECLARATION OF INTERESTS

This project was performed in accordance with the Declaration of Helsinki and approved by the Institutional Review Board of the Shenzhen Third People's Hospital, Shenzhen, China ethics committee (no. 2021-030-08). Written consent was obtained from the participant.

SUPPLEMENTAL INFORMATION

Supplemental information can be found online at https://doi.org/10.1016/j.omton.2026.201251.

REFERENCES

1. Bray, F., Laversanne, M., Sung, H., Ferlay, J., Siegel, R.L., Soerjomataram, I., and Jemal, A. (2024). Global cancer statistics 2022: GLOBOCAN estimates of incidence and mortality worldwide for 36 cancers in 185 countries. CA Cancer J. Clin. *74*, 229–263. https://doi.org/10.3322/caac.21834.
2. Kratzer, T.B., Bandi, P., Freedman, N.D., Smith, R.A., Travis, W.D., Jemal, A., and Siegel, R.L. (2023). Lung cancer statistics. Cancer *130*, 1330–1348. https://doi.org/10.1002/cncr.35128.
3. Siegel, R.L., Miller, K.D., Wagle, N.S., and Jemal, A. (2023). Cancer statistics, 2023. CA Cancer J. Clin. *73*, 17–48. https://doi.org/10.3322/caac.21763.
4. Chan, J.S.K., Tan, M.J., Sng, M.K., Teo, Z., Phua, T., Choo, C.C., Li, L., Zhu, P., and Tan, N.S. (2017). Cancer-associated fibroblasts enact field cancerization by promoting extratumoral oxidative stress. Cell Death Dis. *8*, e2562. https://doi.org/10.1038/cddis.2016.492.
5. Al Bakir, M., Huebner, A., Martínez-Ruiz, C., Grigoriadis, K., Watkins, T.B.K., Pich, O., Moore, D.A., Veeriah, S., Ward, S., Laycock, J., et al. (2023). The evolution of non-small cell lung cancer metastases in TRACERx. Nature *616*, 534–542. https://doi.org/10.1038/s41586-023-05729-x.
6. McGranahan, N., and Swanton, C. (2017). Clonal Heterogeneity and Tumor Evolution: Past, Present, and the Future. Cell *168*, 613–628. https://doi.org/10.1016/j.cell.2017.01.018.
7. Pirlog, R., Cismaru, A., Nutu, A., and Berindan-Neagoe, I. (2021). Field Cancerization in NSCLC: A New Perspective on MicroRNAs in Macrophage Polarization. Int. J. Mol. Sci. *22*, 746. https://doi.org/10.3390/ijms22020746.
8. Kadara, H., Fujimoto, J., Yoo, S.Y., Maki, Y., Gower, A.C., Kabbout, M., Garcia, M.M., Chow, C.W., Chu, Z., Mendoza, G., et al. (2014). Transcriptomic architecture of the adjacent airway field cancerization in non-small cell lung cancer. J. Natl. Cancer Inst. *106*, dju004. https://doi.org/10.1093/jnci/dju004.
9. Kadara, H., and Wistuba, I.I. (2012). Field cancerization in non-small cell lung cancer: implications in disease pathogenesis. Proc. Am. Thorac. Soc. *9*, 38–42. https://doi.org/10.1513/pats.201201-004MS.
10. Liao, Z., Chua, D., and Tan, N.S. (2019). Reactive oxygen species: a volatile driver of field cancerization and metastasis. Mol. Cancer *18*, 65. https://doi.org/10.1186/s12943-019-0961-y.
11. Liao, Z., Tan, Z.W., Zhu, P., and Tan, N.S. (2019). Cancer-associated fibroblasts in tumor microenvironment - Accomplices in tumor malignancy. Cell. Immunol. *343*, 103729. https://doi.org/10.1016/j.cellimm.2017.12.003.
12. Uhlig, J., Case, M.D., Blasberg, J.D., Boffa, D.J., Chiang, A., Gettinger, S.N., and Kim, H.S. (2019). Comparison of Survival Rates After a Combination of Local Treatment and Systemic Therapy vs Systemic Therapy Alone for Treatment of Stage IV Non-Small Cell Lung Cancer. JAMA Netw. Open *2*, e199702. https://doi.org/10.1001/jamanetworkopen.2019.9702.
13. Hanna, N., Johnson, D., Temin, S., Baker, S., Jr., Brahmer, J., Ellis, P.M., Giaccone, G., Hesketh, P.J., Jaiyesimi, I., Leighl, N.B., et al. (2017). Systemic Therapy for Stage IV Non-Small-Cell Lung Cancer: American Society of Clinical Oncology Clinical Practice Guideline Update. J. Clin. Oncol. *35*, 3484–3515. https://doi.org/10.1200/JCO.2017.74.6065.
14. Ashrafi, A., Akter, Z., Modareszadeh, P., Modareszadeh, P., Berisha, E., Alemi, P.S., Chacon Castro, M.D.C., Deese, A.R., and Zhang, L. (2022). Current Landscape of Therapeutic Resistance in Lung Cancer and Promising Strategies to Overcome Resistance. Cancers (Basel) *14*, 4562. https://doi.org/10.3390/cancers14194562.
15. Sosa Iglesias, V., Giuranno, L., Dubois, L.J., Theys, J., and Vooijs, M. (2018). Drug Resistance in Non-Small Cell Lung Cancer: A Potential for NOTCH Targeting? Front. Oncol. *8*, 267. https://doi.org/10.3389/fonc.2018.00267.
16. Kim, J., Koo, B.K., and Knoblich, J.A. (2020). Human organoids: model systems for human biology and medicine. Nat. Rev. Mol. Cell Biol. *21*, 571–584. https://doi.org/10.1038/s41580-020-0259-3.
17. Liao, Z., Lim, J.J.H., Lee, J.X.T., Chua, D., Vos, M.I.G., Yip, Y.S., Too, C.B., Cao, H., Wang, J.K., Shou, Y., et al. (2024). Attenuating Epithelial-to-Mesenchymal Transition in Cancer through Angiopoietin-Like 4 Inhibition in a 3D Tumor Microenvironment Model. Adv. Healthc. Mater. *13*, e2303481. https://doi.org/10.1002/adhm.202303481.
18. Guo, T., Zhang, S., Zeng, W., Liang, Y., Xie, J., Liu, S., Qiu, Y., Fu, Y., Ou, Y., Ma, K., et al. (2024). Isolation and identification of patient-derived liver cancer stem cells and development of personalized treatment strategies. J. Transl. Med. *22*, 1036. https://doi.org/10.1186/s12967-024-05870-9.
19. Cassidy, J.W., Caldas, C., and Bruna, A. (2015). Maintaining Tumor Heterogeneity in Patient-Derived Tumor Xenografts. Cancer Res. *75*, 2963–2968. https://doi.org/10.1158/0008-5472.CAN-15-0727.
20. Sachs, N., Papaspyropoulos, A., Zomer-van Ommen, D.D., Heo, I., Bottinger, L., Klay, D., Weeber, F., Huelsz-Prince, G., Iakobachvili, N., Amatngalim, G.D., et al. (2019). Long-term expanding human airway organoids for disease modeling. EMBO J. *38*, e100300. https://doi.org/10.15252/embj.2018100300.
21. Shi, R., Radulovich, N., Ng, C., Liu, N., Notsuda, H., Cabanero, M., Martins-Filho, S.N., Raghavan, V., Li, Q., Mer, A.S., et al. (2020). Organoid Cultures as Preclinical Models of Non-Small Cell Lung Cancer. Clin. Cancer Res. *26*, 1162–1174. https://doi.org/10.1158/1078-0432.CCR-19-1376.
22. Mazzocchi, A., Dominijanni, A., and Soker, S. (2022). Pleural Effusion Aspirate for Use in 3D Lung Cancer Modeling and Chemotherapy Screening. Methods Mol. Biol. *2394*, 471–483. https://doi.org/10.1007/978-1-0716-1811-0_24.
23. Praharaj, P.P., Bhutia, S.K., Nagrath, S., Bitting, R.L., and Deep, G. (2018). Circulating tumor cell-derived organoids: Current challenges and promises in medical research and precision medicine. Biochim. Biophys. Acta. Rev. Cancer *1869*, 117–127. https://doi.org/10.1016/j.bbcan.2017.12.005.
24. Postel-Vinay, S., and Soria, J.C. (2017). ERCC1 as Predictor of Platinum Benefit in Non-Small-Cell Lung Cancer. J. Clin. Oncol. *35*, 384–386. https://doi.org/10.1200/JCO.2016.70.5053.
25. Wang, Z., Wu, L., Li, B., Cheng, Y., Li, X., Wang, X., Han, L., Wu, X., Fan, Y., Yu, Y., et al. (2023). Toripalimab Plus Chemotherapy for Patients With Treatment-Naive Advanced Non-Small-Cell Lung Cancer: A Multicenter Randomized Phase III Trial (CHOICE-01). J. Clin. Oncol. *41*, 651–663. https://doi.org/10.1200/JCO.22.00727.
26. Hao, Y., Stuart, T., Kowalski, M.H., Choudhary, S., Hoffman, P., Hartman, A., Srivastava, A., Molla, G., Madad, S., Fernandez-Granda, C., and Satija, R. (2024). Dictionary learning for integrative, multimodal and scalable single-cell analysis. Nat. Biotechnol. *42*, 293–304.
27. Jin, S., Guerrero-Juarez, C.F., Zhang, L., Chang, I., Ramos, R., Kuan, C.-H., Myung, P., Plikus, M.V., and Nie, Q. (2021). Inference and analysis of cell-cell communication using CellChat. Nat. Commun. *12*, 1088.
28. Shannon, P., Markiel, A., Ozier, O., Baliga, N.S., Wang, J.T., Ramage, D., Amin, N., Schwikowski, B., and Ideker, T. (2003). Cytoscape: a software environment for integrated models of biomolecular interaction networks. Genome Res. *13*, 2498–2504. https://doi.org/10.1101/gr.1239303.